First demonstration of aerial gamma-ray imaging using drone for prompt radiation survey in Fukushima

Published by IOP Publishing for Sissa Medialab

Received: *September 5, 2017*
Revised: *October 23, 2017*
Accepted: *November 5, 2017*
Published: *November 17, 2017*

First demonstration of aerial gamma-ray imaging using drone for prompt radiation survey in Fukushima

S. Mochizuki,[a,1] **J. Kataoka,**[a] **L. Tagawa,**[a] **Y. Iwamoto,**[a] **H. Okochi,**[a] **N. Katsumi,**[a] **S. Kinno,**[a] **M. Arimoto,**[a] **T. Maruhashi,**[a] **K. Fujieda,**[a] **T. Kurihara**[a] **and S. Ohsuka**[b]

[a] *Research Institute for Science and Engineering, Waseda University, Shinjuku, Tokyo 169-8555, Japan*
[b] *Central Research Laboratory, Hamamatsu Photonics K.K., Hamamatsu, Shizuoka, Japan*

E-mail: mosaku39@fuji.waseda.jp

Abstract: Considerable amounts of radioactive substances (mainly ^{137}Cs and ^{134}Cs) were released into the environment after the Japanese nuclear disaster in 2011. Some restrictions on residence areas were lifted in April 2017, owing to the successive and effective decontamination operations. However, the distribution of radioactive substances in vast areas of mountain, forest and satoyama close to the city is still unknown; thus, decontamination operations in such areas are being hampered. In this paper, we report on the first aerial gamma-ray imaging of a schoolyard in Fukushima using a drone that carries a high sensitivity Compton camera. We show that the distribution of ^{137}Cs in regions with a diameter of several tens to a hundred meters can be imaged with a typical resolution of 2–5 m within a 10–20 min flights duration. The aerial gamma-ray images taken 10 m and 20 m above the ground are qualitatively consistent with a dose map reconstructed from the ground-based measurements using a survey meter. Although further quantification is needed for the distance and air-absorption corrections to derive *in situ* dose map, such an aerial drone system can reduce measurement time by a factor of ten and is suitable for place where ground-based measurement are difficult.

Keywords: Dosimetry concepts and apparatus; Photon detectors for UV, visible and IR photons (solid-state) (PIN diodes, APDs, Si-PMTs, G-APDs, CCDs, EBCCDs, EMCCDs etc); Scintillators, scintillation and light emission processes (solid, gas and liquid scintillators)

[1] Corresponding author.

https://doi.org/10.1088/1748-0221/12/11/P11014

2017 JINST 12 P11014

Contents

2017 JINST 12 P11014

1 Introduction

After the nuclear disaster of Fukushima Daiichi Nuclear Power Plant (NPP), decontamination operations were effectively implemented but are still limited to the city or farmland near the residential area. However, more than 70% of Fukushima prefecture is covered by forest, wherein a large but unknown amount of radioactive substances is still being accumulated. A series of dose maps have been provided by the Japan Atomic Energy Agency (JAEA) based on aerial monitoring at an altitude of 150–300 m, which covers almost all the contaminated fields in Fukushima [1, 2]. To obtain higher resolution images, JAEA further developed an unmanned helicopter system that can hover and fly at an altitude of 10–150 m [3, 4]. The measurement results from November 2013 to October 2016 are open to public, but limited to a local area within a 5 km radius from the Fukushima Daiichi NPP [5]. Moreover, the air dose rate was measured using a $LaBr_3$(Ce) scintillation detector with no directionality; thus, the spatial resolution is limited to 160 m for a fixed flight altitude 80 m and a track width of 80 m. Apparently, this spatial resolution is not sufficient for evacuees who hope to return to their hometown. Ideally, a spatial resolution as good as a few meters is required to find local hotspots in residential areas, especially near private houses [6, 7].

In addition, such radiation survey should be conducted regularly even after the decontamination operations are completed. This is because the radioactive substances may flow out with the rainwater from the satoyama (undeveloped woodland near populated area) to residential areas; thus, distribution may vary with time. In order to find local hotspots of radiation sources in a city or in private houses, ground-based measurements using gamma-ray visualization modules are being

proposed. One of the configurations, a pinhole camera, is the easiest way of imaging gamma rays but needs heavy collimator [8]. Moreover, the detector efficiency is limited by geometrical area of a pinhole, which must be as small as possible to achieve good angular resolution. In this context, another methods, using a Compton camera, is advantageous, as it utilizes the kinematics of Compton scattering instead of mechanical collimator to provide a source image [9, 10]. Examples of ground-based field tests using various Compton cameras in restricted areas of Fukushima can be found in literature [11–19]. However, an aerial survey is the most effective method to determine the distribution of radioactive substances in a forest, satoyama or even in the crowded regions downtown. Prototypical tests using an unmanned helicopter have been reported but are not widespread, partly because of high cost (∼1M USD) and large size (3.63 m long; 94 kg weight) of the helicopter necessary to carry a bulky detector systems [4, 5]. We also note that, aerial gamma ray imaging and spectroscopy are also necessary in the field of homeland security and geological research, from mining and hydrocarbon exploration to the construction industry [20–22].

In this paper, we proposed a novel and alternative aerial system using a commercial drone, DJI S1000+, which is relatively cheaper than the conventional system (∼6000 USD) and compact (∼1.0 m diagonal wheelbase; 4.2 kg weight). The disadvantage with using such a small drone is that the maximum payload and flight time is limited to ∼5 kg and 10 min, respectively, as compared to those of unmanned helicopter (e.g., ∼10 kg and 90 min for the case of above [3]). Therefore, we have to ensure all the detector systems are compact and light weight. In addition, we have to develop dedicated wireless communication systems between the drone and ground station. Additionally, gamma-ray camera with a high sensitivity is required so that an aerial dose map can be obtained within a single short flight of 10 min. Here we present the first results of aerial gamma-ray imaging by mounting a compact Compton camera (1.9 kg weight [12]) onboard a drone in Namie, Fukushima. We confirm that aerial snapshots are qualitatively consistent with the dose map reconstructed from the ground-based measurements with substantial reduction in the measurement time by a factor of 10.

2 Ground-based measurements

2.1 Methods

The experiment site was a schoolyard in the Tsushima branch of Namie high school in Namie-city, Fukushima, located at 37°33′45″ N, 140°46′7″ E. Prior to the experiment using a drone, we created an air dose rate map of the entire schoolyard to determine the distribution of radioactive substances, namely ^{137}Cs. As shown in figure 1, the schoolyard is surrounded by pine forests and many young pine trees are also growing near the boundary, but only few are seen in the center of the schoolyard. We defined 6×5 points that are 20 m apart that cover a 100 m (longitudinal) × 80 m (lateral) region of the schoolyard. Around each measurement point, we measured the air dose rate ten times at 30 cm height from the ground by choosing a position randomly within a 2 m radius from the center. We used a scintillator-based survey meter (Gamma Spotter; FURUKAWA CO., LTD), and adopted average values. The measurement time is 5 min × 30 points and an additional 30 min for the walking time. Note that deviations of ten measurements were all within 10% for each point.

2017 JINST 12 P11014

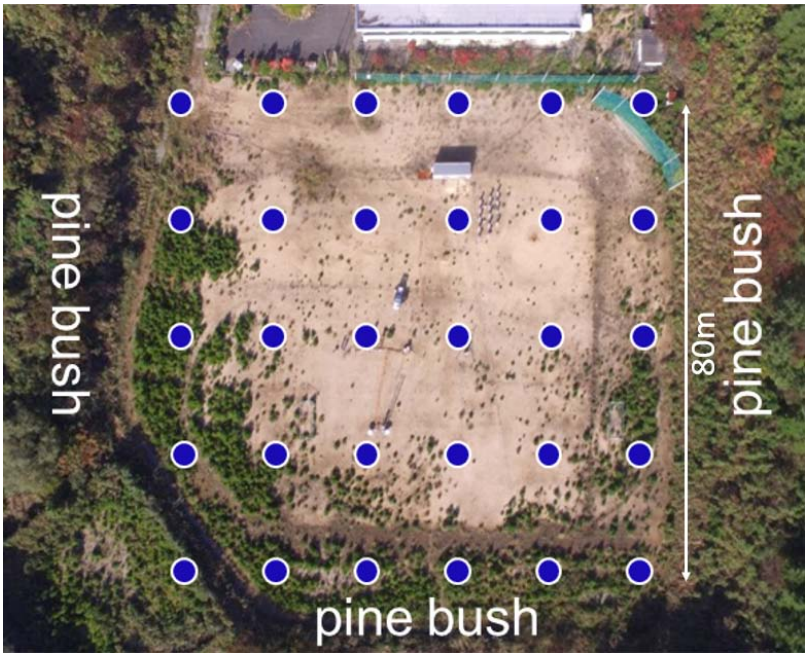

Figure 1. An aerial photograph of the schoolyard of Tsushima branch of Namie high school in Namie-city, Fukushima. The schoolyard is surrounded by pine bushes near the boundary. We defined 6×5 points as shown in the figure for the ground based measuments of radiation dose rate, that are 20 m apart that cover a 100 m × 80 m region of the schoolyard.

2.2 Results

Figure 2 shows a radiation dose map reconstructed from ground-based measurements. The total time spent for the measurements was more than 3 hours. To derive a continuous two-dimensional (2D) map, the air dose rate at an arbitrary point in the schoolyard was calculated by applying spline interpolation of data at 30 sampling positions. However, ^{137}Cs is often concentrated within narrow regions of a few meters in size in the region of Fukushima [14, 15]. Therefore, we may have missed some local hotspots, localized between the sampling points, during the ground-based measurements. Although 30 measurements points are too few to determine the dose distribution over the schoolyard, we must consider the fact that the survey time becomes unreasonably longer as number of points increased. Therefore, such sparse sampling of the schoolyard can be considered as just a reference and hence, may not be correct especially when local hotspots exist somewhere between the measurement points. In this context, observation using a drone could provide fair and accurate dose maps without missing any hotspots in the same field of view.

3 Gamma-ray snapshot using a drone

3.1 Methods

3.1.1 Compact Compton camera

The Compton camera utilizes the kinematics of Compton scattering to contract the source image without using mechanical collimators or coded masks. It also features a wide field of view. The

2017 JINST 12 P11014

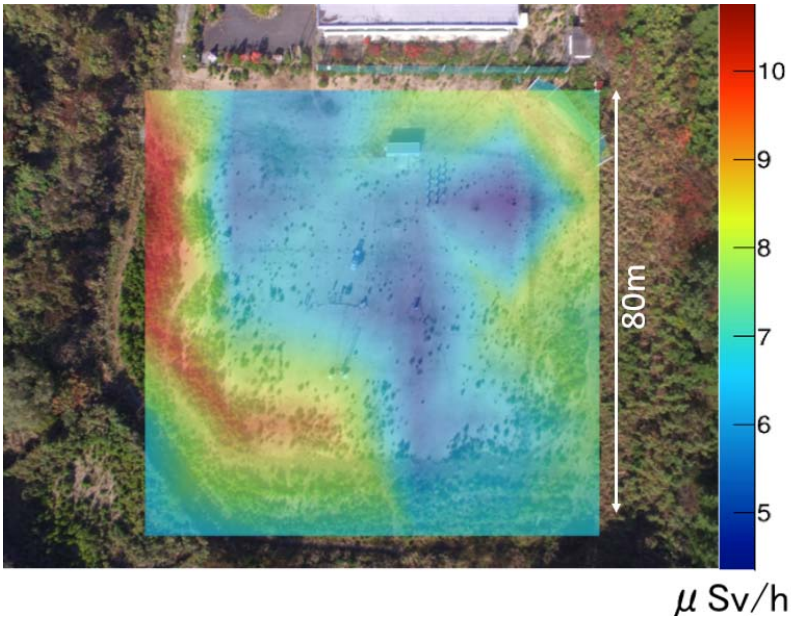

Figure 2. Air dose rate map of the schoolyard reconstructed from the spline interpolation of ground-based measurements at 30 sampling points using a scintillator-based survey meter. Color scale indicates the dose rate in units of μSv/h. The total measurement time was 180 min.

camera consists of two or more layers, namey, the scatterer and absorber. When a gamma-ray photon is scattered in one detector and absorbed in another, the incident energy of gamma ray E_0, is clearly a sum of E_1 and E_2, where E_1 denotes the energy of the recoil electron and E_2 is the energy of the scattered photon. Furthermore, the scattering angle θ is calculated as:

$$\cos\theta = 1 - \frac{m_e c^2}{E_2} + \frac{m_e c2}{E_1 + E_2} \tag{3.1}$$

in which the source image can be extracted as a superposition of multiple Compton cones [13, 14].

Due to limited payload of a commercial drone, gamma-ray visualization module must be compact and light weight. Moreover, the detector must be very sensitive so that reliable gamma-ray images can be obtained within a short flight duration of ~10 min. A Compton camera (shown in figure 3) that we developed with Hamamatsu Photonics in 2013 is most effective and suitable for this purpuse. The Compton camera weighs only 1.9 kg and is ~13.5×14×15 cm^3 in size [10]. It also has fisheye lens, and provides both the visual image and gamma-ray images are provided in real time. This camera has already been used many times in Fukushima for ground based measurements as detailed in literature [13–16].

Our Compton camera consists of a scatterer and absorber, both of which have Ce:$Gd_3(Al,Ga)_5O_{12}$ (Ce:GAGG) [23, 24] scintillator arrays optically coupled to an MPPC (Multi-Pixel Photon Counter) array. Note that Ce:GAGG has excellent characteristics such as high density (6.63 g/cm^3), high light yield (60,000 photon/MeV), non-deliquescence and no internal background radiation. Thus the sensitivity of the Compton camera is very high such that a 1 MBq ^{137}Cs source positioned at 50 cm from the camera can be imaged within 10 sec, which corresponds to 0.35 μSv/h

2017 JINST 12 P11014

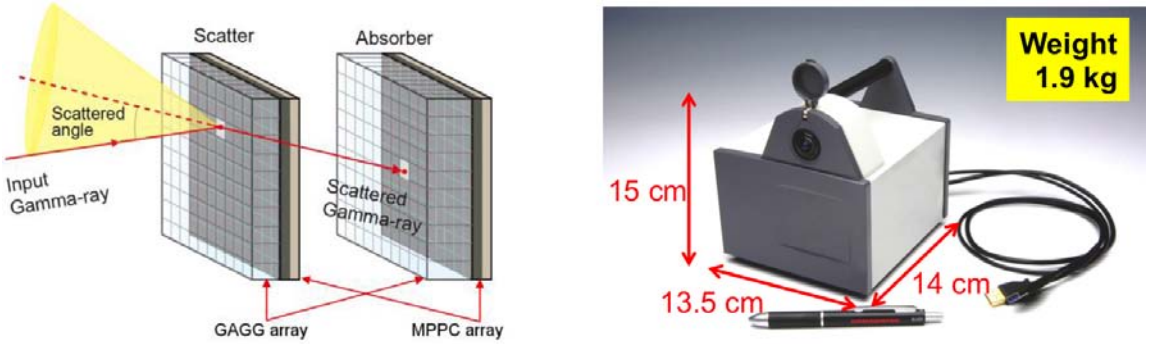

Figure 3. (*left*) Concept of Compton camera imaging by using the scatterer and the absorber. Full details are given in the text. (*right*) Photo of a handheld Compton camera on a drone.

at camera position. The angular resolution of the camera is $\Delta\theta \simeq 14$ deg (FWHM) and the energy resolution is 9% (FWHM) as measured with 662 keV gamma rays.

3.1.2 Drone and flight system

The drone used (Spreading Wings S1000+) was obtained from DJI products; it is very easy to use and need only 5 min of preparation before it is ready to fly. Though the diagonal wheel base is 104.5cm long, it has a high portability because the arm can be folded during transportation. It weighs 4.4 kg and the maximum payload is 11 kg. Thus considering the weight of the battery (2.0 kg for 6S 20,000 mAh), the net payload allowed for the detector system is 4.6 kg. Although the maximum flight time with a 20,000 mAh battery is 15 min, the flight time depends on the weight of payload; thus, it is desirable to reduce the load to extend the flight time as much as possible. As for the attitude control system, we installed a GPS, accelerometer, and speedometer. GPS acquires the latitude, longitude and altitude of the drone, and the accelerometer and speedometer acquires the respective values in the three axial directions. When these sensors are properly used, the hovering accuracy is 1.5 m in the horizontal direction and 0.5 m in the height direction. However, we will directly measure the pointing accuracy later in section 4.1. The maximum wireless communication range is 1.2 km between the drone and the ground station.

While the Compton camera itself is light enough, substantial modification are necessary to achieve wireless communication between the Compton camera and a ground station. We employed various options based on USB over IP via card CPU (Raspberry Pi, Intel Edison), however, the data acquisition system was frequently interrupted owing to unstable power supply. Hence, we decided to put both the Compton camera and the notebook PC (~2 kg) onboard, and to share the screen data between the notebook and the ground station via virtual network computing as shown in figure 4. As a result, the final loading rate of the system was about 85%.

3.1.3 Gamma-ray snapshots using a drone

The Compton camera provides a fish-eye view of visual and gamma-ray images using the equisolid angle projection method. This is a convenient method for conventional ground-based surveys in which the distance is unknown but the direction of hotspots to the camera can be defined. We

2017 JINST 12 P11014

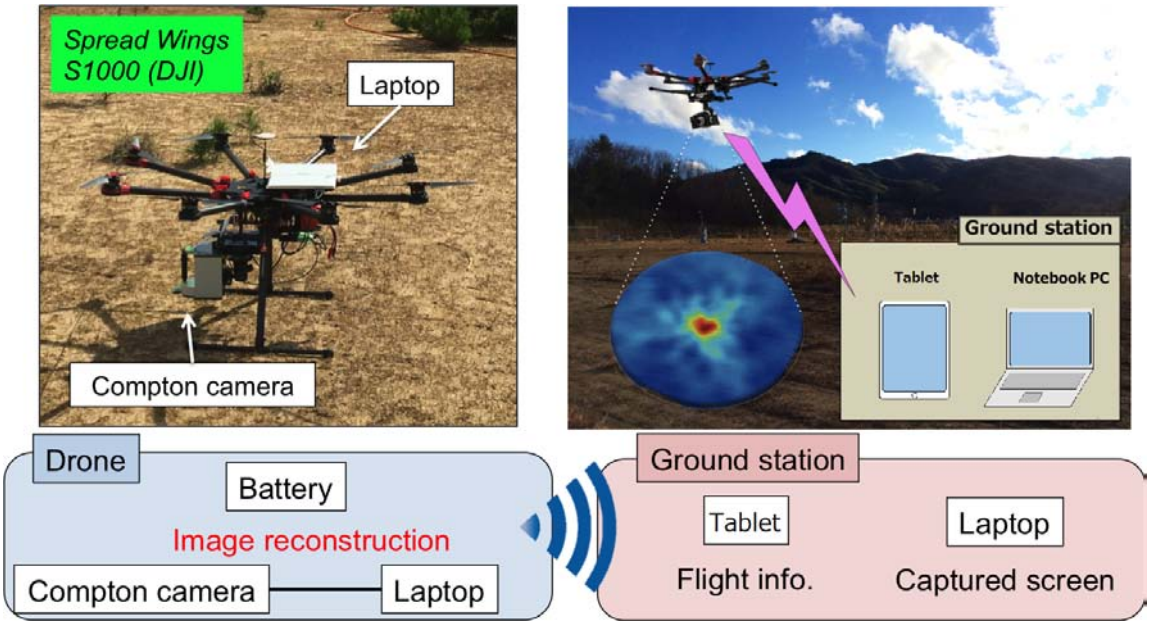

Figure 4. (*upper left*) Photo of the drone with the Compton camera attached to it prior to the flight. (*upper right*) Conceptual design of flight measurements and (*bottom*) wireless communication system between the drone and the ground station.

constructed aerial gamma-ray images in real time by applying simple back projection. This is a very simple imaging method of gamma rays that projects the Compton cone obtained by Compton kinematics onto the unitary spherical surface. Since the sensitivity of the Compton camera depends on the direction of the incident gamma rays, corrections were made by dividing a raw image with an invert of sensitivity map over the field of view. The maximum likelihood-expectation maximization (MLEM) algorithm in the list mode was applied to the image as detailed in references [13].

In order to determine the distribution of radioactive substances over the entire schoolyard, which is 100 m long in both the longitudinal and lateral direction, we first divide the schoolyard into four subsets as shown in figure 5 Here the field center of each flight is shown as a *yellow* star, whereas the entire filed of view of 50 m diameter is shown as *yellowed* dashed circle. Then, at each flight point, the drone hovers at a target altitude of 10 m and makes measurements with a Compton camera. The gamma-ray images are reconstructed with the energy selection criteria of $10\,\mathrm{keV} < E_1 < 165\,\mathrm{keV}$ and $612 < E_1 + E_2 < 712\,\mathrm{keV}$, where E_1 and E_2 are the energy deposits in the scatterer and absorber (see, equation (3.1)) to match with the photon energy of ^{137}Cs. Simultaneously a fisheye camera mounted on the Compton camera was used to shoot a video of the forward 140 degrees field of view. This video can be utilizes for evaluating the attitude fluctuation as shown in section 4.1.

3.2 Results

3.2.1 Aerial imaging from 10 m above the ground

Figure 6 compares the visible and gamma-ray images (662 keV from ^{137}Cs) taken with a compact Compton camera onboard a drone, reconstructed from four aerial snapshots at a target altitude of 10 m. Note that the all images presented here are from the fisheye view to emphasize the advantage

2017 JINST 12 P11014

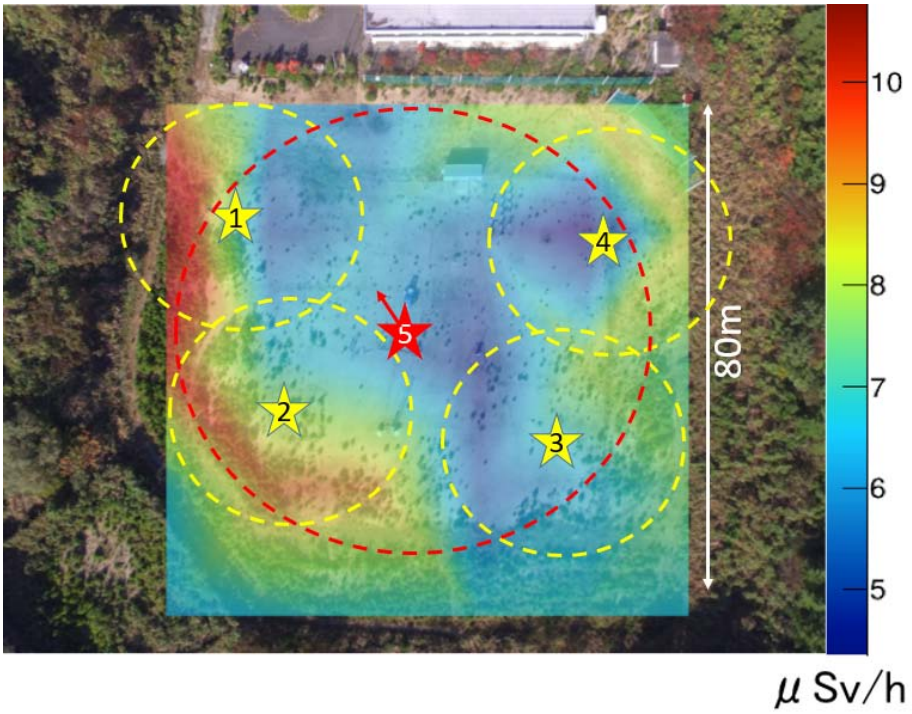

Figure 5. Pointing positions of aerial snapshots using a drone. *Yellow* stars indicate the center of the field of view for Flight 1–4 at a target altitude of 10 m (see, table 1 for more details). *Yellow* dashes show a circle with a 50 m diameter corresponding to the field of view of the Compton camera. *Red* stars and dashes indicate the center and the field of view of Flight 5 at an altitude of 20 m.

Table 1. Acquisition time and number of 662 keV events accumulated to reconstruct images for Flight 1-4.

Flight Num.	1	2	3	4
Flight time	13m17s	11m40s	13m36s	14m7s
Num. of reconstruction events	880	1011	667	505

of the wide field of view of the Compton camera (140 deg). The sensitivity of the detector depends on the incident direction of gamma rays; thus it is corrected over the field of view. The detailed flight information and accumulated number of 662 keV events for each flight are listed in table 1. Figure 6 shows the intensity of gamma-ray images normalized using the length of each flight time (measurement time). Thus, the relative intensity, shown in arbitrary units, is proportional to the count per sec (cps) of detected gamma rays and can be directly compared. These aerial gamma-ray images clearly indicate that the left side of the schoolyard in Flight 1 and 2 shows a high dose rate, tracing the distribution of pine trees, which is consistent with the ground-based measurements in figure 2. A slight mismatch between aerial dose map and ground-based measurements in Flight 4 is probably due to hotspots, which are relatively weak compared to those in Flight 1 and 2, and are located near the field of view thus lager distance to the Compton camera. The angular resolution of the Compton camera is 14 deg (FWHM) at 662 keV, corresponding spatial resolution ranges from 2 m (field center) to 5 m (edge of field of view) in the same image.

2017 JINST 12 P11014

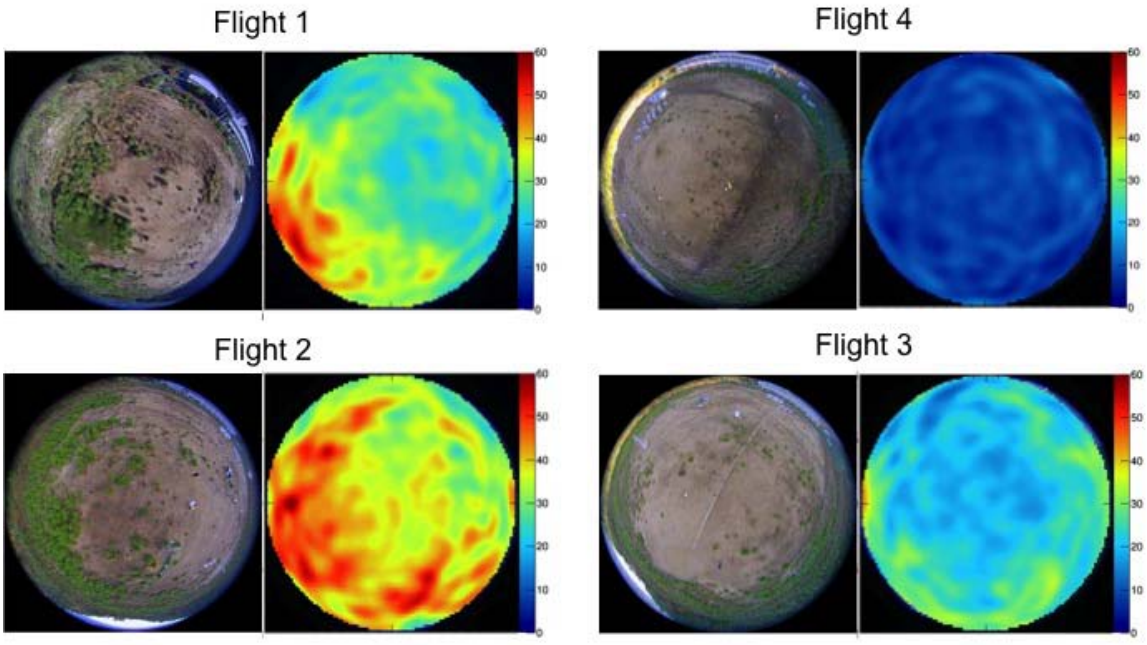

Figure 6. Comparison of fisheye visual image (*left*) and gamma-ray snapshots (*right*) obtained 10 m above the ground using a drone for Flight 1 to Flight 4. The units of color-bar are arbitrary but normalized with the measurement time.

Table 2. Acquisition time and number of 662 keV events accumulated to reconstruct images for Flight 5.

Flight Num.	5-a	5-b	5-a+5-b
Flight time	11m43s	13m26s	25m9s
Num. of reconstruction events	146	330	476

3.2.2 Aerial imaging from 20 m above the ground

Larger regions can be observed at a once when flight altitude is becoming higher altitude, at the expense of reduced gamma-ray events that can be used for image reconstruction. Thus to determine the maximum flight altitude at which meaningful images can be obtained during a short flight of ~10 min, we tried a hovering flight at 20 m twice. The flight center and direction of field of view were the same for these two flights, which are shown by the *red* star and dashed circles (100 m diameter) in figure 5. Again, the gamma-ray images obtained at 20 m converge to the pine bush on the left, as shown in figure 7, which is consistent with the results obtained at 10 m. The results were combined for two measurements to increase the photon statistics. The number of reconstructed events for 662 keV gamma rays was 476 and the total measurement time was 25 min and 9 sec. The detailed flight information and accumulated number of 662 keV events for each flight are listed in table 2. Note that the upper right of the image shows a weak hotspot as indicated in the ground-based measurements. The spatial resolution for the 20 m snapshot ranges from 4 m to 10 m, depending on the location in the field of view.

2017 JINST 12 P11014

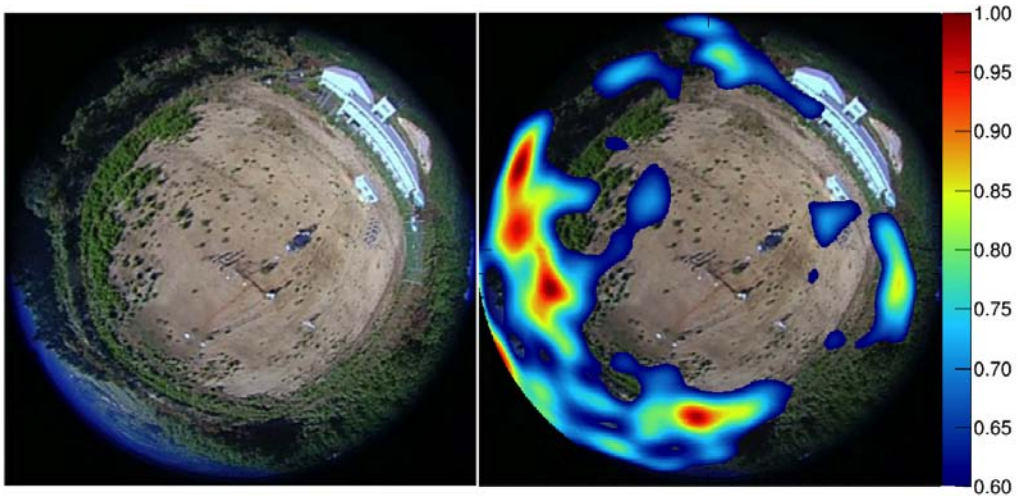

Figure 7. Comparison of fisheye visible image (*left*) and gamma-ray snapshots (*right*) obtained 20 m above the ground using a drone for Flight 5.

4 Discussion

4.1 Evaluation of pointing accuracy

While we tried to fix the pointing position using the GPS, a drone equipped with a Compton camera was constantly moving in the sky to keep the same position, especially owing to the influence of wind during a hovering flight. In order to evaluate effects of such fluctuation on an image, we used a fisheye camera mounted on a Compton camera to record a video. As shown in figure 8 (*left*), we set arbitrary marker in the video and traced the pixel ID of this maker for each picture frame. Then the fluctuation of the pixel ID is converted to the angle deviation. Figure 8 (*right*) shows a histogram of θ (opening angle) and ϕ (rotation angle) during a flight. The deviations of θ and ϕ were 2.3 degrees and 1.8 degrees, respectively. These pointing fluctuations cause blurring of gamma-ray image to 1.7 degree, which is negligible compared to angular resolution of 14 degree as measured at 662 keV gamma rays.

The altitude of the drone is measured either by GPS or laser range finders, both of which have an uncertainty of 1–2 m, which is slightly larger than hovering accuracy of 50 cm as described above. Hence, in addition to distance effect as discussed above, we suspect that the altitude of Flight 4 may be a bit higher than expected, around 11–12 m. This may also account for a slight mismatch in the relative intensity between the aerial dose map and ground based measurements.

4.2 Statistical fluctuation in the image

In general, gamma-ray images are strongly affected by low photon statistics. Therefore, any apparent structures observed in the gamma-ray images might be artifacts due to a relatively poor number of events used to reconstruct an image. We therefore need to know the amount of photons required to construct a reliable image. Figure 9 (*upper*) shows variation in gamma-ray images as a result of increasing the number of reconstruction events by 100 events for Flight 2. For simplicity, we increased the photon statistics by increasing the exposure time of the recorded dataset in Flight 2, to reach

2017 JINST 12 P11014

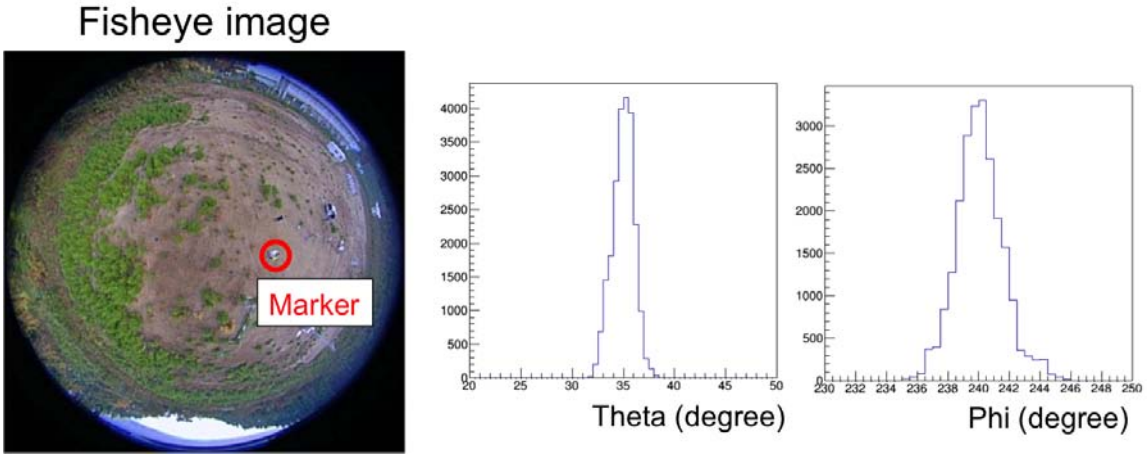

Figure 8. (*left*) Position marker used in the flight measurements. (*right*) Example of pointing flucutation during a single flight of 10 min.

the requested photon counts between 100 and 1000. We used the simple back-projection method to obtain the images. It shows that the image does not change significantly above 500 events. For a more quantitative analysis, we can evaluate the minimum number of events required for convergence by using the normalized mean squared error (NMSE) method. The NMSE method normalizes the mean square error of the evaluation image with respect to the reference image as follows:

$$\mathrm{NMSE} = \frac{\sum(g(x,y) - f(x,y))^2}{\sum f(x,y)^2}, \tag{4.1}$$

where $f(x, y)$ denotes the reference image and $g(x, y)$ denotes the test image. The NMSE value approaches zero as the evaluation image approaches the reference image. From figure 9 (*lower*), we conclude that ~500 events should be the minimum number of events for which the NMSE converged. Thus, as shown in table 1, a sufficient number of events is obtained for all measurements presented in this paper.

4.3 Works for future

While aerial mapping using a drone is a convenient and powerful tool to find local hotspots quickly, gamma-ray images, as shown in figure 5 and 6, are given an arbitrary unit and thus, are difficult to directly compare with ground-based measurements, such as those shown in figure 2. There are likely two missing pieces to convert the arbitrary unit into the absolute dose rate values: (1) estimating the distance to the region of interests (ROIs) in the images taken with the Compton camera, which were obtained using the equisolid angle projection method (see section 3.1) and (2) measuring the integrated radiation dose at camera positions of either 10 m or 20 m above the ground, then redistributing the dose to be consistent with the distance and relative color scale given by the arbitrary unit. Ideally, the distance to the subject (i.e., a certain point in the schoolyard) can be derived in aerial mapping as a function of the flight altitude of the drone; thus, projection onto the image plane seems to be more convenient than onto the spherical surface. This is, however, not easy because the intensity (count rates of gamma rays) of every image pixel must be corrected in

2017 JINST 12 P11014

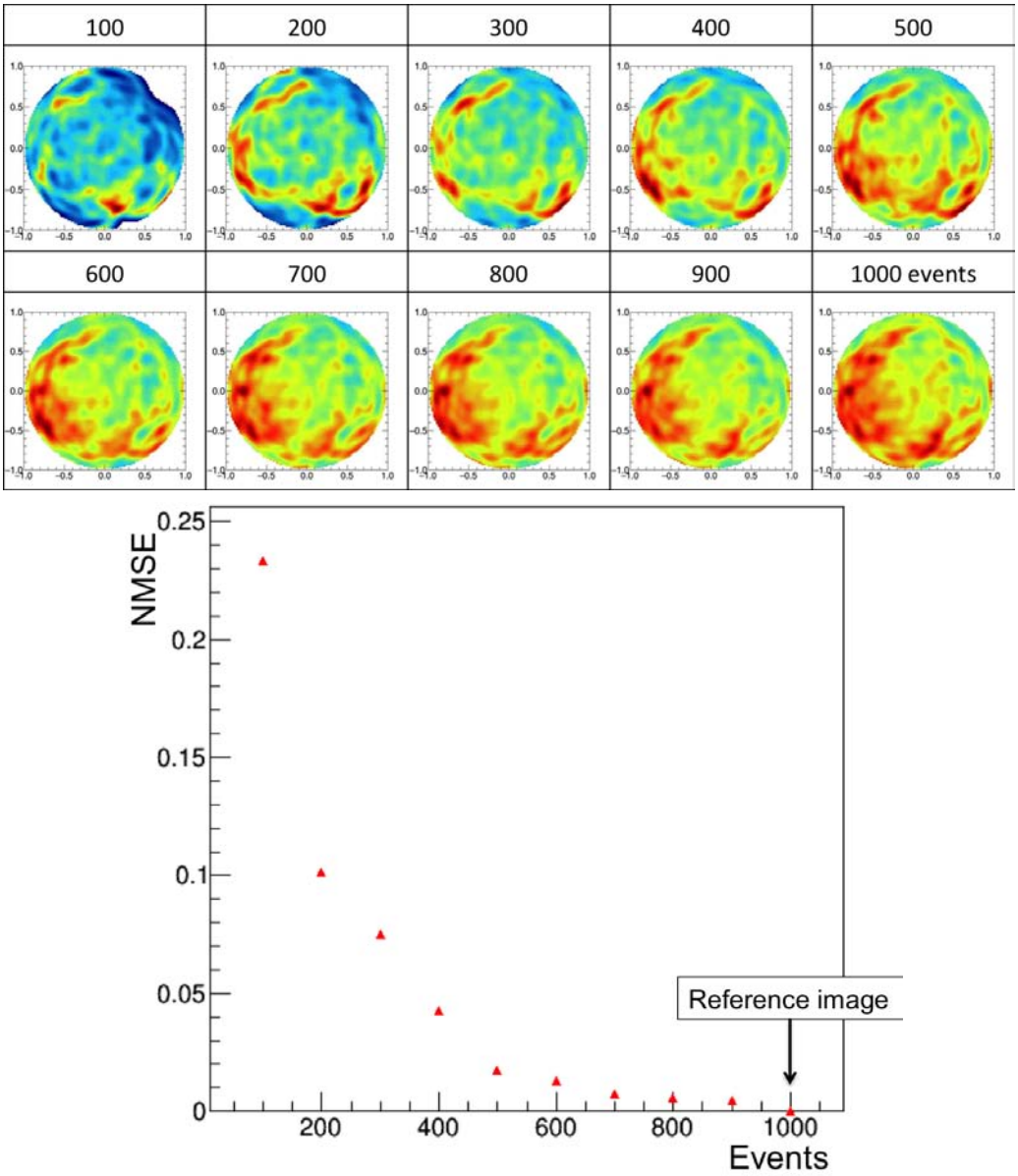

Figure 9. (*upper*) Variations of reconstructed gamma-ray images with increasing photon statistics during Flight 2. For simplicity, we increased the photon statistics by increasing the exposure time of the recorded dataset in Flight2, to reach the requested photon count between 100 and 1000. (*lower*) NMSE as a function of number of events suggesting that the minimum number of required events is 500 for gamma-ray images to converge. See text for more details.

our case according to the distance and air absorption. Moreover, in general, the subject may not be as flat as a schoolyard, especially for in the case of mountains, forests and satoyamas. Therefore in this study, we limit ourselves to only raw gamma-ray images reconstructed using the usual method of equisolid angle projection without any corrections, but the results still qualitatively agree with the ground-based measurements. In the next step, we develop a new Compton camera system with 3D distance measurement sensors, which will be reported on in future work.

2017 JINST 12 P11014

We also note that the accuracy of the flight altitude system, typically 1–2 m, was not sufficient, as detailed in section 4.1. To improve the altitude control and measurement system, we installed D-RTK GNSS (Global Navigation Satellite System), which is a revised navigation system specifically designed for a drone DJI S1000+, although a detailed performance test is still in progress. In this context, exhaustive studies of altimetric measurements using low-cost GNSS, and radar and barometer sensors are reported, emphasizing the effectiveness of cheap and light barometric sensors [25]. Connecting the Compton camera and such a GNSS is a subject of future work.

5 Conclusion

In this paper, we proposed a novel method of using a commercial drone for aerial gamma-ray imaging, which carries a handheld Compton camera developed for environmental survey in Fukushima, Japan. We showed that the obtained images, taken from 10m and 20m above the ground, are qualitatively consistent with the ground-based measurements. In particular, high dose regions tracing the distribution of pine trees are successfully imaged within 10 or 20 min, reducing the measument time by a factor of 10. While such aerial imaging is a convenient and powerful way to find local hotspots, which are difficult to find in random sampling on the ground-based survey, current aerial mapping provides only a relative intensity of ^{137}Cs in arbitrary units, thus preventing direct comparison to ground-based measurement. Moreover, we note that the accuracy of the flight altitude system may severely affect the resultant images taken with the drone. As a next step, we will implement a revised altitude control system for a drone featuring a high precision GNSS. In addition, we are developng a dedicated method to convert the obtained Compton camera images, taken with an arbitrary unit, into absolute dose rate values.

Acknowledgments

The authors acknowledge the referee for a careful reading and for a number of useful and positive suggestions that helped to improve the manuscript. This work was supported by JSPS KAKENHI Grant Number JP15H05720.

References

[1] S. Okuyama et al., *A Remote Radiation Monitoring System Using an Autonomous Unmanned Helicopter for Nuclear Emergencies*, *J. Nucl. Sci. Technol. Suppl.* **5** (2008) 414.

[2] Y. Sanada and T. Torii, *Aerial radiation monitoring around the Fukushima Dai-ichi nuclear power plant using an unmanned helicopter*, *J. Environ. Radioactiv.* **139** (2015) 294.

[3] J. Jiang et al., *A prototype of aerial radiation monitoring system using an unmanned helicopter mounting a GAGG scintillator Compton camera*, *J. Nucl. Sci. Technol.* **53** (2016) 1067.

[4] Y. Shikaze et al., *Field test around Fukushima Daiichi nuclear power plant site using improved* $Ce:Gd_3(Al,Ga)_5O_{12}$ *scintillator Compton camera mounted on an unmanned helicopter*, *J. Nucl. Sci. Technol.* **53** (2016) 1907.

[5] http://emdb.jaea.go.jp/emdb/en/portals/b225/.

2017 JINST 12 P11014

[6] A. Haefner et al., *Handheld real-time volumetric 3-D gamma-ray imaging*, *Nucl. Instrum. Meth.* **A 875** (2017) 42.

[7] K. Vetter et al., *Gamma-Ray imaging for nuclear security and safety: Towards 3-D gamma-ray vision*, *Nucl. Instrum. Meth.* **A** (2017), in press.

[8] F.J. Beekman and F.V. der Have, *The pinhole: gateway to ultra-high-resolution three-dimensional radionuclide imaging*, *Eur. J. Nucl. Med. Mol. Imag.* **34** (2007) 151.

[9] V. Schönfelder, A. Hirner and K. Schneider, *A telescope for soft gamma ray astronomy*, *Nucl. Instrum. Meth.* **107** (1973) 385.

[10] R.W. Todd, J.M. Nightingale and D.B. Evertt, *A proposed γ camera*, *Nature* **251** (1974) 132.

[11] S. Takeda et al., *A portable Si/CdTe Compton camera and its applications to the visualization of radioactive substances*, *Nucl. Instrum. Meth.* **A 787** (2015) 207.

[12] J. Kataoka et al., *Handy Compton camera using 3D position-sensitive scintillators coupled with large-area monolithic MPPC arrays*, *Nucl. Instrum. Meth.* **A 732** (2013) 403.

[13] J. Kataoka et al., *Recent progress of MPPC-based scintillation detectors in high precision X-ray and gamma-ray imaging*, *Nucl. Instrum. Meth.* **A 784** (2015) 248.

[14] A. Kishimoto et al., *Performance and field tests of a handheld Compton camera using 3-D position-sensitive scintillators coupled to multi-pixel photon counter arrays*, 2014 *JINST* **9** P11025.

[15] T. Nishiyama et al., *A novel Compton camera design featuring a rear-panel shield for substantial noise reduction in gamma-ray images*, 2014 *JINST* **9** C12031.

[16] K. Takeuchi et al., *Stereo Compton cameras for the 3-D localization of radioisotopes*, *Nucl. Instrum. Meth.* **A 765** (2014) 187.

[17] M. Kagaya et al., *Development of a low-cost-high-sensitivity Compton camera using CsI (Tl) scintillators (γI)*, *Nucl. Instrum. Meth.* **A 804** (2015) 25.

[18] D. Tomono et al., *First On-Site True Gamma-Ray Imaging-Spectroscopy of Contamination near Fukushima Plant*, *Sci. Rept.* **7** (2017) 41972.

[19] T. Tanimori et al., *Establishment of Imaging Spectroscopy of Nuclear Gamma-Rays based on Geometrical Optics*, *Sci. Rept.* **7** (2017) 415111.

[20] K. Kamada et al., *Composition engineering in cerium-doped* $(Lu, Gd)_3(Ga, Al)_5O_{12}$ *single-crystal scintillators*, *Cryst. Growth Des.* **11** (2011) 4484.

[21] Furukawa Co. Ltd., http://www.furukawakk.co.jp/pdf/others/hikaku.pdf (in Japanese).

[22] M.A.S. Youssef and S.T. Elkhodary , *Utilization of airborne gamma ray spectrometric data for geological mapping, radioactive mineral exploration and environmental monitoring of southeastern Aswan city, South Eastern Desert, Egypt*, *Geophys. J. Int.* **195** (2013) 1689.

[23] A.G. Darnley and K.L. Ford, *Regional Airborne Gamma-Ray Surveys: A Review*, in *Exploration '87 Proceedings*, pg. 229–240 (1987).

[24] G. Burgada et al., *A segmented detector for airborne gamma ray spectroscopy*, in *International Joint Conference RADIO 2014*, Gramado, RS, Brazil, 26–29 Augustl 2014.

[25] M. Albéri et al., *Accuracy of Flight Altitude Measured with Low-Cost GNSS, Radar and Barometer Sensors: Implications for Airborne Radiometric Surveys*, *Sensors* **17** (2017) 1889.

2017 JINST 12 P11014